

Relationships between the integrity and function of lumbar nerve roots as assessed by diffusion tensor imaging and neurophysiology

S. Y. Chiou¹ · P. J. Hellyer^{2,3} · D. J. Sharp² · R. D. Newbould⁴ · M. C. Patel⁵ · P. H. Strutton¹

Received: 7 February 2017 / Accepted: 14 June 2017
© The Author(s) 2017. This article is an open access publication

Abstract

Purpose Diffusion tensor imaging (DTI) has shown promise in the measurement of peripheral nerve integrity, although the optimal way to apply the technique for the study of lumbar spinal nerves is unclear. The aims of this study are to use an improved DTI acquisition to investigate lumbar nerve root integrity and correlate this with functional measures using neurophysiology.

Methods Twenty healthy volunteers underwent 3 T DTI of the L5/S1 area. Regions of interest were applied to L5 and S1 nerve roots, and DTI metrics (fractional anisotropy, mean, axial and radial diffusivity) were derived. Neurophysiological measures were obtained from muscles innervated by L5/S1 nerves; these included the slope of motor-evoked potential input-output curves, F-wave latency, maximal motor response, and central and peripheral motor conduction times.

Results DTI metrics were similar between the left and right sides and between vertebral levels. Conversely, significant differences in DTI measures were seen along the course of the nerves. Regression analyses revealed that DTI metrics of

the L5 nerve correlated with neurophysiological measures from the muscle innervated by it.

Conclusion The current findings suggest that DTI has the potential to be used for assessing lumbar spinal nerve integrity and that parameters derived from DTI provide quantitative information which reflects their function.

Keywords Diffusion tensor imaging · Nerve integrity · Spinal nerve roots · Transcranial magnetic stimulation · Electrical stimulation · Neurophysiology

Introduction

Diffusion tensor imaging (DTI) can be used to characterise the microstructure of tissue in vivo [1]. It has been applied in the central nervous system (CNS), and studies have shown the clinical application of using DTI in the evaluation and diagnosis of a number of conditions including stroke, traumatic brain injury, and multiple sclerosis [2–5]. Recent work has demonstrated the feasibility of using DTI to measure the integrity of peripheral nerves [6–9], and a recent meta-analysis suggests that fractional anisotropy (FA) may be a useful measure of median nerve structure in patients with carpal tunnel syndrome (CTS) [10].

Compression of lower lumbar spinal nerves caused by herniation of the intervertebral disc is a common condition, with a prevalence of 10 to 25% in Europe [11]; the incidence peaks occur in the fifth decade. It can lead to severe pain in the legs (sciatica) and lower back as well as functional disability, which place enormous burden on health services [12, 13]. Spinal surgery is often performed to relieve leg pain if conservative treatment is not successful and pain persists into chronicity; the outcome of surgery, however, is highly variable [14]. Currently, the primary diagnostic indicator for the

✉ P. H. Strutton
p.strutton@imperial.ac.uk

¹ The Nick Davey Laboratory, Division of Surgery, Human Performance Group, Department of Surgery and Cancer, Faculty of Medicine, Imperial College London, London, UK

² Computational, Cognitive and Clinical Neuroimaging Laboratory, Division of Brain Sciences, Imperial College London, London, UK

³ Department of Bioengineering, Imperial College London, London, UK

⁴ Imanova, Ltd, London, UK

⁵ Imaging Department, Imperial College Healthcare NHS Trust, Charing Cross Hospital, London, UK

surgical decision-making process is spinal magnetic resonance imaging (MRI), but discrepancies between symptoms and MRI findings are frequently observed [15, 16]. Although conventional MRI can be used to determine the location of nerve compression, it does not permit prediction of the effects of treatment, as the extent of nerve damage is difficult to estimate.

DTI has the potential to complement standard MRI, as it provides a quantitative measure of tissue microstructure and nerve integrity [17]. However, DTI of the lumbar spine is challenging, given the relatively small cross-sectional area of the lumbar nerve roots, the presence of susceptibility artefacts around the spinal cord due to tissue-bone interfaces and the co-localisation of large stores of body fat [18, 19]. Despite these challenges, initial work using DTI and tractography to visualise and evaluate these nerves in healthy subjects and in patients with lumbar nerve compression has shown promising results. Lower fractional anisotropy (FA) and higher mean diffusivity (MD) or apparent diffusion coefficient (ADC) have been observed in compressed nerve roots, compared to both contralateral uncompressed nerve roots and equivalent nerve roots in healthy subjects [20–23].

The function of nerve roots can be assessed using neurophysiology, and this, combined with DTI, provides an opportunity to test the degree to which alteration in nerve integrity relates to function. Work in the central nervous system shows correlations between diffusion metrics and neurophysiological measures. For example, corpus callosum DTI parameters correlate with interhemispheric inhibition measured by paired-pulse transcranial magnetic stimulation (TMS) [24], suggesting that structural abnormalities demonstrated by DTI have a functional impact. The function of lumbar spinal nerves is routinely assessed using neurophysiological testing (e.g. nerve conduction studies) and is altered in patients with radiculopathy [25–27]. However, whether measures of nerve microstructure assessed using DTI reflect function in these nerves remains to be established.

In this study, we first examine whether the diffusion metrics derived from our optimised DTI acquisition are comparable between sides and across nerves. Fibre-tracking was also applied to test whether the tractography fibre bundle can be tracked and matched to the lumbar nerve roots on the T2-weighted MRI images. Next, we investigated the relationships between lumbar spinal nerve integrity (measured using DTI) and function (using neurophysiological measurements) of the nerve roots (and muscles innervated by) L5 and S1 in healthy subjects; lumbar disc herniation most frequently compresses these nerve roots. Specifically, we test the hypothesis that measures of microstructure such as FA, MD, axial and radial diffusivity (AD and RD) correlate with neurophysiological measurements reflecting the function of the peripheral nervous system (e.g. F-wave latency).

Materials and methods

Participants

With ethical approval and written informed consent, 20 healthy adults (12 male; mean \pm SD age, 33.3 ± 8.91 years; height, 1.71 ± 0.10 m) were recruited from students and staff at the authors' institution. Participants were excluded if they had a history of musculoskeletal abnormalities of the back musculature, axial skeleton or lower limbs (e.g. low back pain, radiculopathy). Further, exclusion criteria related to the use of TMS and of MRI (i.e. metal implants, cardiac pacemaker, history of epilepsy or fits, previous brain injury, neurosurgery, neurological disorders, psychological disorders, actively taking antidepressants or other neuromodulatory drugs).

MRI data acquisition

All MRI data were collected using a 3T Siemens Verio clinical MRI scanner (Siemens Healthcare, Erlangen Germany). Subjects were imaged supine using an 11 cm local loop coil centred over the intervertebral disc between L5 and S1 in combination with two elements of the phased-array spine coil to maximise the signal-to-noise ratio in the lumbar roots to further improve the diffusion imaging. Correct coil positioning was verified by initial localizer scans. Structural imaging was reviewed by a consultant radiologist to confirm no evidence of lumbar nerve compression; this included sagittal T1-weighted (T1w) and T2-weighted (T2w) turbo spin echo (TSE), coronal T2w TSE, as well as a multislab T2w TSE angled axially to the L3-L4, L4-L5, and L5-S1 vertebral discs. Diffusion-weighted images (DWI) were acquired with $b = 800$ s/mm² using a twice-refocused diffusion preparation, an inverted slice select gradient on the refocusing pulses for improved fat saturation [28], and a 2D EPI readout. Forty 2.5 mm thick adjacent slices of a 100×256 mm field of view (FOV) were collected with TE = 92 ms, TR = 9 s and 50×128 resolution with readout bandwidth of 1562 Hz per pixel, giving a resolution of $2.0 \times 2.0 \times 2.5$ mm. The effectiveness of using a reduced phase-encoding field of view (FoV) to reduce susceptibility-induced distortions in lumbar nerve imaging has been demonstrated [19, 29]. Saturation bands were placed superiorly and inferiorly to the imaging slab to reduce flow and off-resonance excitation artefacts. Sixty-four non-collinear directions interspersed with a $b = 0$ measurement after every 16 directions were collected resulting in 68 acquisitions in 10 m:21 s.

Neurophysiological measurements

Recording Electromyographic (EMG) recordings were obtained bilaterally from the target muscles, tibialis anterior (TA) and soleus (SOL). Pairs of Ag/AgCl electrodes (self-

adhesive, 2 cm diameter, CareFusion, UK) were positioned parallel to the muscle fibre orientation. A ground electrode was placed over the left lateral malleolus. For TA, electrodes were positioned at one third way down a line between the head of the fibula and the superior aspect of the medial malleolus; for SOL, two-thirds way down a line between the medial condyle of the femur and the medial malleolus. Participants were additionally asked to contract the target muscles by ankle dorsiflexion or plantarflexion to confirm that the electrodes were located over the most prominent muscle bulk. EMG data were filtered (10–1000 Hz), amplified (1000×; Iso-DAM, World Precision Instruments, UK) and sampled at 2 kHz using a Power 1401 data acquisition system and Signal v5 software (Cambridge Electronic Design [CED], UK) connected to a computer for subsequent offline analysis.

TMS TMS was delivered to the motor cortex using a Magstim 200² mono-phasic stimulator (The Magstim Company Ltd., UK) connected to a figure-of-eight coil (wing outer diameter 10 cm), positioned over the approximate location of primary motor cortex at a site which elicited a maximal motor-evoked potential (MEP) in the contralateral target muscle.

Experimental parameters Measurements were conducted, while participants were seated in an armchair with torso supported by the backrest and feet strapped securely on a wood plate on the floor. Three brief (~2 s) maximum voluntary contractions (MVC), with at least 10 s rest between contractions, were recorded from each target muscle; strong verbal encouragement was provided throughout. The mean rectified EMG over 500 ms during each of the three MVCs was calculated and averaged, and 10% of this value was displayed continuously on a screen as visual feedback for participants during all TMS measurements.

Corticospinal excitability Measurements were performed on each target muscle separately and while participants maintained contraction levels at 10% MVC of the target muscle. Active motor threshold (AMT) was established for each target muscle, which was defined as the lowest intensity of TMS that evoked visible MEPs in at least three of six consecutive trials. Motor-evoked potentials (MEPs) were evoked by TMS, and an input-output relationship of MEP amplitude to stimulus intensity (IO curve) was constructed. Stimulus intensities started at 10% below the AMT and were increased in 10% steps of AMT until the intensity reached to the maximal device output. Intensities were randomised and six MEPs at each intensity were recorded. TMS pulses were given every 8 s with several periods of rest given to participants between trials to avoid muscle fatigue.

M-wave and F-waves A maximal motor response (M_{\max}) and F-waves were measured with the use of supramaximal stimuli via a cathode to the common peroneal nerve around the fibular

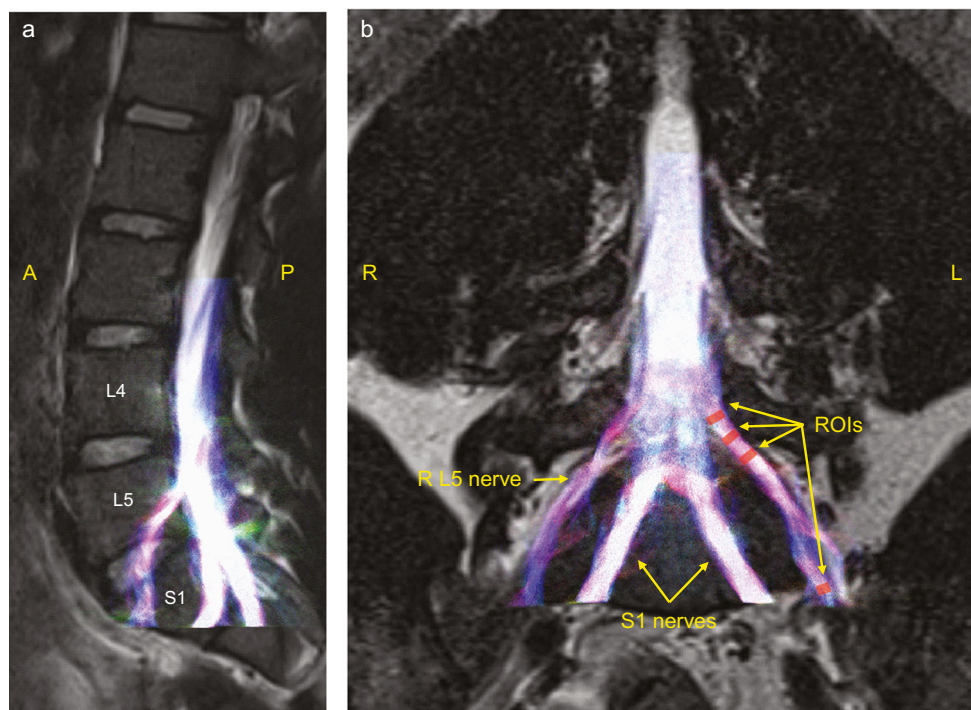
head (for TA) or the tibial nerve in the popliteal fossa (for SOL) (Digitimer DS7, Digitimer UK, 500- μ s pulse duration). The anode was placed over the patella on the stimulated side. Five M_{\max} at the same intensity were recorded; an intensity of 120% of the intensity used to elicit M_{\max} was delivered to the nerve at 1 Hz until 20 F-waves were recorded.

Data analysis

DTI Post-processing of diffusion-weighted images (DWI) and fitting of the diffusion tensor were performed using the FSL Diffusion Toolbox (FDT) (FSL, <http://fsl.fmrib.ox.ac.uk/fsl>) v.5.0.6 (Oxford, UK). The diffusion tensor was estimated using the FSP Diffusion Toolkit [30, 31]. Fractional anisotropy (FA), mean diffusivity (MD) and axial diffusivity (AD) maps were generated using FDT as well as voxel-wise estimates for each of the eigenvalues (λ_1 , λ_2 and λ_3) representing the magnitude of diffusion in the three principal directions. Radial (RD) diffusivity images were then derived from the eigenvalues ($RD = \lambda_2 + \lambda_3/2$). In order to evaluate these measures along the course of each of the L5 and S1 nerves on both the left and right side, a region of interest (ROI) approach was used. ROIs were manually drawn with reference to the axial view of $b = 0$ image from the diffusion acquisition overlaid onto the co-acquired axial T2-weighted image (see Fig. 1). Three binary ROIs were manually traced onto the image using FSLview (FSL, <http://fsl.fmrib.ox.ac.uk/fsl>) on both left and right L5 and S1 nerves below the disc ~14, ~20 and ~28 mm distal to the centre of the disc. A fourth ROI was placed over the most distal visible portion of the nerve visible within the field of view. Due to the close proximity of the L5 nerve to the central spinal canal, it was difficult to place with any degree of accuracy any ROIs above the level of the disc. However, for the S1 nerves, where clear differentiation could be made between nerve above the level of the disc and the spinal canal, an additional ROI was placed immediately above (within 2.5 mm of) the disc. Each ROI was drawn to cover the entire visible signal on the $b = 0$ image which was clearly differentiable as nerve, resulting in ROIs of between 40 and 60 mm³ (with a slice thickness of 2.5 mm, this equates to 16 and 24 mm², respectively). This size of ROI reduces the partial volume effect; the neutral-position cross-sectional area of nerve roots in the lower lumbar region has been shown in a cadaveric study to be 34.48 ± 11.25 mm² [32]. This manual ROI drawing generated a total of eight binary ROI masks. For each of the FA, MD, AD and RD images, ROI diffusion values were sampled from over-lapping voxels between each of the masks and the metric of interest. The average of each metric within each mask was subsequently taken forward into further analysis.

Fibre tracking For visualisation, basic fibre tracking analysis was performed at the level of each of the L5 and S1 spinal

Fig. 1 Overlaid diffusion tensor tractography of L5 and S1 nerves on the T2-weighted sagittal (a) and coronal (b) images of the lumbar spine from a representative subject. Tractography shows the anatomical orientation of L5 and S1 nerves. The mean orientation of the streamlines is indicated in colours: left-right (red), anterior-posterior (green) and inferior-superior (blue). Regions of interests as described in the “Methods” are illustrated for the left L5 nerve. The regions of interest (ROIs) from proximal to distal for the L5 nerve are at ~14, ~20 and ~28 mm inferior to the disc and at the distal end of the nerve. R right, L left, A anterior, P posterior



nerves. Fibre orientation distribution (FOD) analysis and fibre tracking were performed on the DWI data using MRtrix (<https://github.com/MRtrix3/mrtrix3>). Voxelwise FODs were estimated using constrained spherical deconvolution [33], with an lmax of 6. Probabilistic tractography was performed the iFOD2 algorithm [33], with a step size of half the DWI voxel size, a turning angle threshold of 90° and an streamline termination threshold of FOD < 0.1. Tracks were seeded from the spinal canal superior to the L5 and S1 nerves, and terminated on entering the most distal ROI in each of the bilateral L5 and S1 nerves (see above). Streamlines were seeded at random from the seed until 10,000 streamlines successfully traversed from the seed to each of the target ROIs.

EMG The mean MEP amplitude per stimulus intensity was calculated and normalised to the M_{\max} for each muscle; this was defined as MEP_{max}. The mean MEP amplitudes between 110 and 170%AMT and between 110 and 140%AMT were used to calculate slopes for the TA and SOL, respectively; the slopes (IO_{slope}) were defined as the steepness of the linear regression line for the given data points [34]. Mean pre-stimulus EMG was calculated in a 100-ms window from the rectified EMG traces for the TA and SOL at each intensity. The average rectified EMG trace from the trials in which 120% AMT was delivered was used to derive the MEP latency for each muscle. The amplitude and latency of averaged M_{\max} were measured, and the minimum latency of F-waves was identified from the recorded 20 F-waves. Central motor

conduction time (CMCT) and peripheral motor conduction time (PMCT) were calculated using the following equations:

$$CMCT(ms) = MEP\ latency - \left(\frac{Mmax\ latency + min.F\ wave\ latency - 1}{2} \right)$$

$$PMCT(ms) = \frac{Mmax\ latency + min.F\ wave\ latency - 1}{2}$$

Statistical analysis

Data were analysed using SPSS 21 (IBM Corp, Armonk, NY). To fully describe the relationship between nerve “Level” (L5 vs. S1), “Side” (left vs. right) and “ROI” (four ROIs distal to the disc) in healthy controls, repeated measures ANOVA with post hoc *t* tests were used. The same analysis was carried out to examine the effect of “Intensity” and “Side” on IO curves and pre-stimulus EMG for the TA and SOL. Paired *t* tests were used to examine side differences on IO_{slope}, M_{\max} , minimum F-wave latency, CMCT and PMCT. To establish a relationship between DTI parameters and neurophysiological measurements, regression analysis was employed for DTI metrics of L5 and S1 separately with the neurophysiological measurements obtained from their corresponding muscles. The DTI parameters from the ROI closest to the level of the disc were used in this analysis. Neurophysiological parameters were IO_{slope}, M_{\max} , minimum F-wave latency, CMCT and PMCT. Age, gender and body

height were included as covariates of no interest. Statistical significance was set at $p < 0.05$, and Bonferroni correction was applied to adjust for multiple comparisons. Further, Pearson correlation coefficient analyses were performed on DTI metrics and TMS parameters to examine any correlation between L5 and S1 nerves and between TA and SOL. Data are presented as mean \pm SD in the text and as mean \pm SEM in the figures.

Results

DTI and fibre tracking of lumbar nerve roots

The lumbar nerve roots were well visualised in the diffusion-weighted acquisitions, and fibre tracking was successful in all 20 subjects. A representative dataset is shown in Fig. 1, demonstrating the excellent co-localization between the geometrically accurate TSE and the optimised diffusion-weighted EPI that is well-known for geometric distortion. Table 1 shows DTI parameters. FA, MD, AD and RD values were very similar between left and right sides, showing no significant side differences. Further, there were no significant differences between vertebral levels (L5 and S1) in these measures.

Changes in DTI metrics along the course of the nerve

The diffusion metrics were significantly different along the course of the nerve with FA increasing in proximal-to-distal, and MD, AD and RD decreasing (Fig. 2). Post hoc paired t tests showed that the FA obtained from the most proximal portions of the nerves was significantly lower than that from the others ($p < 0.05$). The paired t tests showed that the MD, AD and RD obtained from the most proximal portions of the nerves were higher than that from the other ROIs ($p < 0.05$).

Within-subject variation in neurophysiological measurements

The normalised amplitudes of MEPs in both TA and SOL increased with increasing stimulus intensity (both $p < 0.05$), but there were no laterality differences (Fig. 3). Additionally, there were no laterality differences in the slope of input-output curves of MEP amplitude against stimulus intensity (IO_{slope}),

maximal motor response (M_{max}), minimum F-wave latency, and central and peripheral motor conduction time (CMCT and PMCT) in either TA or SOL (Table 2).

L5 DTI metrics correlate with maximal motor response and latency

Since there were no laterality differences in DTI metrics or neurophysiological measurements, data from left and right sides were averaged prior to regression analyses. Regression analysis showed that the DTI metrics correlated with the function of the peripheral nerves. Specifically, L5 FA was correlated with the amplitude of maximal motor response (M_{max}) obtained from TA, the effector muscle of L5 (overall $F_{4,15} = 8.72$; $p = 0.001$; partial correlation $r = 0.51$, $p = 0.037$; Fig. 4a). In addition, both MD (overall $F_{4,15} = 7.63$; $p = 0.001$; partial correlation $r = -0.5$, $p = 0.039$; Fig. 4b) and AD (overall $F_{4,15} = 7.64$; $p = 0.001$; partial correlation $r = -0.51$, $p = 0.039$; Fig. 4c) of L5 were correlated with the minimum F-wave latency obtained from TA. There were no correlations between S1 DTI metrics and neurophysiological measurements from SOL.

Discussion

In the present study, DTI parameters of lumbar spinal nerves and their relationships with neurophysiological measures were investigated in healthy subjects. The DTI metrics derived from our diffusion imaging were consistent across left and right sides of the nerves at a given level, between L5 and S1 levels at a particular location, and across individuals even though the number of subject was limited. In addition, tractography of L5 and S1 nerves was successfully obtained and well localised to the lumbar nerves on the T2-weighted MRI. These suggest that our optimised DTI acquisition can provide stable DTI measures; a study to determine if they detect abnormalities in clinical populations is currently in progress. In addition, our results suggest that the integrity of the lumbar spinal nerves was different along the course of the nerve. FA increased from proximal to distal, while MD, AD and RD decreased. Further, we show that the MD and AD of the L5 nerve correlated with the minimum F-wave latency measured from the TA muscle, while the FA correlated with the

Table 1 Diffusion tensor imaging (DTI) metrics and results of statistical analyses

| DTI metric | Level (L5, S1) | Side (left, right) | ROI (~14, ~20, ~28 mm, distal) |
|------------|--------------------------------|---------------------------------|----------------------------------|
| FA | $F_{1,14} = 0.39$; $p = 0.54$ | $F_{1,14} = 0.15$; $p = 0.71$ | $F_{3,42} = 9.42$; $p < 0.001$ |
| MD | $F_{1,14} = 1.69$; $p = 0.21$ | $F_{1,14} = 0.04$; $p = 0.85$ | $F_{3,42} = 15.27$; $p < 0.001$ |
| AD | $F_{1,14} = 1.05$; $p = 0.32$ | $F_{1,14} = 0.008$; $p = 0.93$ | $F_{3,42} = 14.58$; $p < 0.001$ |
| RD | $F_{1,14} = 1.86$; $p = 0.20$ | $F_{1,14} = 0.05$; $p = 0.82$ | $F_{3,42} = 15.15$; $p < 0.001$ |

FA fractional anisotropy, MD mean diffusivity, AD axial diffusivity, RD radial diffusivity, ROI region of interest

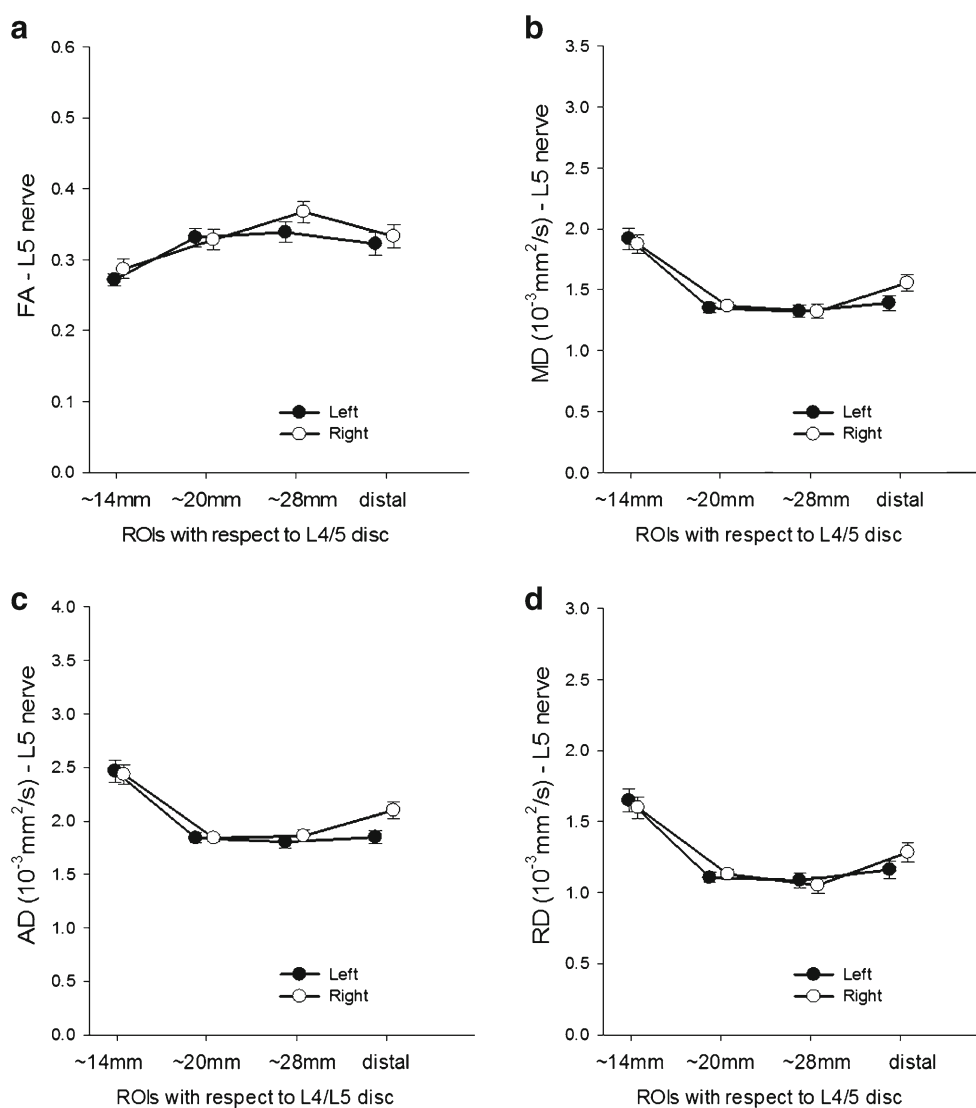


Fig. 2 Diffusion tensor imaging (DTI) metrics along the course of the left and right L5 (a–d) and S1 (e–h) nerves. Data are presented as mean \pm standard error

amplitude of maximum motor response of the TA. The current findings provide a preliminary set of normative values of diffusion metrics for L5 and S1 nerves and show that the metrics, at least at L5, reflect the function of the nerves.

The feasibility of using diffusion MRI to derive DTI parameters from lumbar spinal nerves has been reported previously [20–22, 35, 36]. The majority of those studies measured DTI values at a single location of the nerves and reported no differences in FA, MD and ADC between left and right sides of the nerves as well as between L5 and S1 levels in healthy subjects. Only one of these studies [35] used multiple ROIs to characterise FA and ADC values along the course of the L5 and S1 nerve roots. Their findings, from a small sample of six healthy subjects, showed that FA increased distally from the junction of the dura mater while the ADC decreased. DTI acquisitions in the lumbar spine are compromised by poor magnetic field homogeneity. This results in spatially varying

chemically selective (fat) saturation and pronounced geometric image distortion. Prior studies have relied on full field of view acquisitions. Reduction in the phase-encoding FOV linearly decreases the geometric distortion in that direction. The readout direction uses a high readout bandwidth that is often two orders of magnitude higher than that in the phase-encoding direction. A reduced phase-encoding FOV is essential for lumbar DTI [20]. Robust fat saturation was achieved in this study by using an inverted slice selection gradient on the refocusing pulses, not used in any of the previous studies. The majority of prior studies used chemically selective saturation of the fat signal, which fails in the presence of magnetic field inhomogeneities as expected here. Some prior studies utilised fat-selective inversion to improve fat saturation [20, 22]; however, that technique is sensitive to both field and RF inhomogeneities. Our work substantiates and extends previous work by using a multiple ROI approach on the L5 and S1 nerve

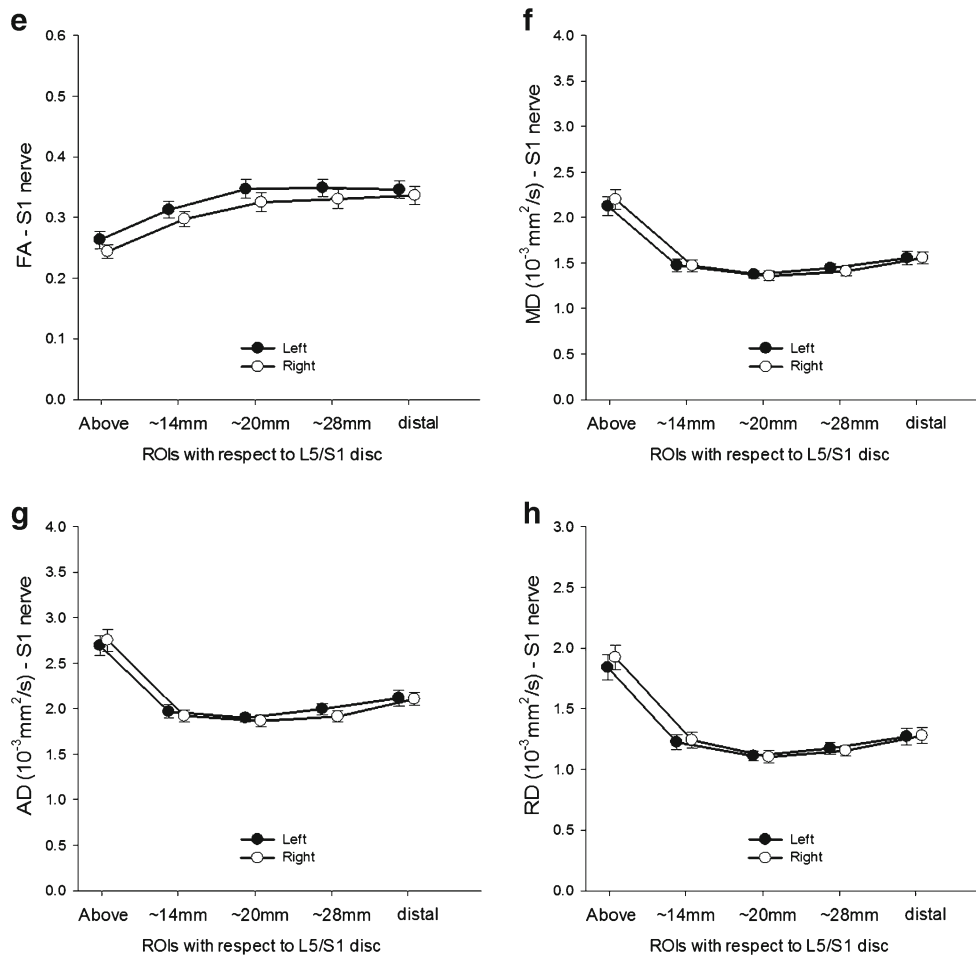


Fig. 2 (continued)

roots in a preliminary cohort of 20 healthy subjects and, in addition to deriving FA and MD, also calculated AD and RD, which reflect perpendicular and parallel diffusivity, respectively. Our results show increases in FA in a proximal to distal direction and decreases in MD, AD and RD with little variation between sides and levels (L5, S1). This suggests that our imaging approach might be able to detect subtle changes occurring in L5 and S1 nerves which could be useful in

monitoring surgical recovery in patient populations and warrants further investigation in a larger cohort.

Changes in DTI metrics along a proximo-distal course have been reported previously for the median nerve in the forearm, wrist and hand in healthy subjects, with a minimum FA in the centre of the carpal tunnel and maximum MD and RD values at the same location [37]. The authors suggested that the reduction in FA in the median nerve as it crosses the carpal tunnel

Fig. 3 Input-output curves of motor-evoked potentials (MEP) from tibialis anterior (TA; **a**) and soleus (**b**) that display mean MEP amplitude on the y-axis against the stimulus intensity on the x-axis. The MEP amplitude was normalised to M_{max} , and the stimulus intensity was expressed as the percentage of active motor threshold (AMT). Data are presented as mean \pm standard error

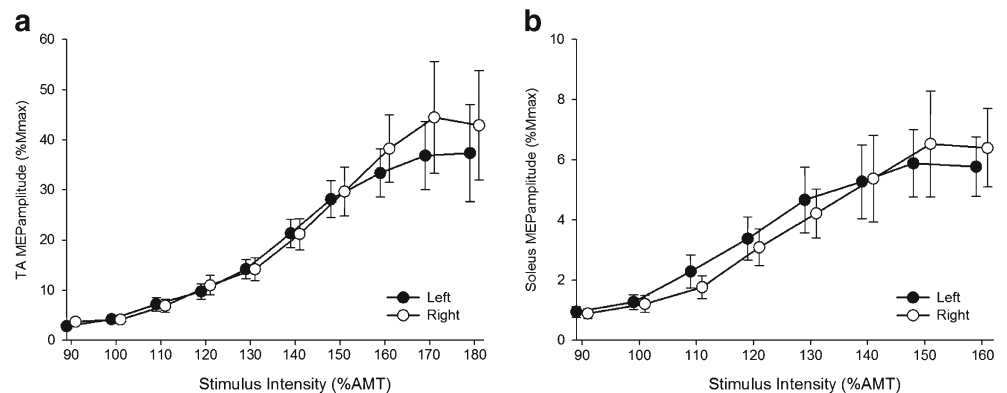


Table 2 Neurophysiological parameters and results of statistical analyses

| Parameter | Tibialis anterior | | | Soleus | | |
|-------------------------------------|-------------------|--------------|----------------|--------------|--------------|----------------|
| | Left | Right | <i>p</i> value | Left | Right | <i>p</i> value |
| IO curve slope (MEP amplitude/%AMT) | 1.28 ± 0.95 | 1.46 ± 1.12 | 0.50 | 0.26 ± 0.30 | 0.26 ± 0.24 | 0.94 |
| M_{max} (mV) | 4.97 ± 2.02 | 5.60 ± 2.32 | 0.19 | 12.62 ± 8.58 | 11.81 ± 7.19 | 0.62 |
| Minimum F-wave latency (ms) | 34.40 ± 3.77 | 35.21 ± 3.47 | 0.11 | 32.01 ± 3.21 | 32.21 ± 2.20 | 0.68 |
| CMCT (ms) | 12.74 ± 2.13 | 12.18 ± 2.72 | 0.13 | 13.85 ± 3.21 | 14.00 ± 3.03 | 0.84 |
| PMCT (ms) | 18.04 ± 1.91 | 18.33 ± 1.80 | 0.28 | 17.32 ± 1.20 | 17.45 ± 1.22 | 0.59 |

Data are presented as mean ± standard deviation

IO curve input-output curve, MSO maximal stimulate output, M_{max} maximal motor response, CMCT central motor conduction time, PMCT peripheral motor conduction time

reflects a possible entrapment site. The lumbar nerve roots are frequently compressed by herniated discs or narrowing foramina, and studies have shown that FA and ADC or MD are altered, with decreases in FA and/or increases in ADC or MD, in the compressed roots in comparison with the

uncompressed roots [20–23, 38, 39]. Lower FA and/or higher ADC or MD in the compressed nerve roots suggest changes in diffusion direction and an increase in water diffusion which might indicate altered microstructure occurring in the compressed nerve. These findings show clinical utility of DTI to

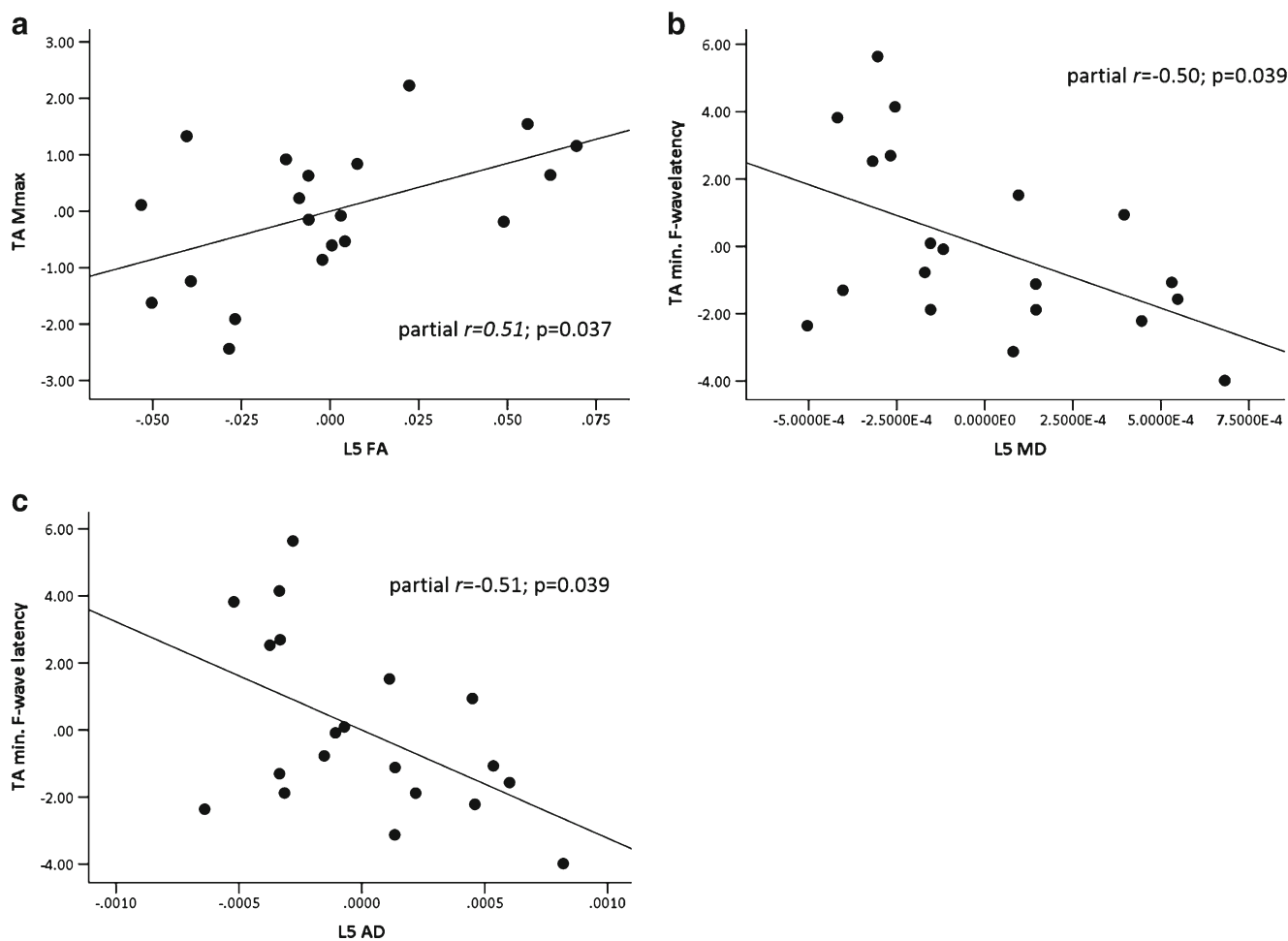


Fig. 4 Relationships between DTI metrics of L5 and neurophysiological measurements obtained from the tibialis anterior (TA). Partial regression plots showing **a** fractional anisotropy (FA) correlated with the M_{max} , **b** mean diffusivity and **c** axial diffusivity both correlated with minimum F-

wave latency. The x- and y-scales of the partial correlation plots represent the adjusted values of DTI metrics and neurophysiological measurements after including age, gender and height as covariants

detect nerve impingement caused by a number of spinal pathologies, such as intervertebral disc herniation, degenerative disc disease, foraminal stenosis and spondylolisthesis.

It is not well established which features of nerve structure are revealed by DTI measures; functional assessment, e.g. using neurophysiological testing, is therefore required. Our results show that MD and AD in L5 root correlated with the minimum F-wave latency, reflecting conduction time along the nerve [40], from stimulation of the common fibular nerve, while the FA in the L5 root correlated with the maximum motor response (M_{\max}). The increase in MD (often called ADC) has been shown to be associated with increased tissue water levels caused by inflammation in multiple sclerosis [41, 42] or oedema in cerebral cancer [43]; however, correlations with neurophysiological function in these clinical populations are unclear. Studies on the median nerve have shown correlations between MD and nerve conduction velocities in patients with carpal tunnel syndrome, substantiating our current findings. Further, our results of a correlation between FA and M_{\max} are consistent with some previous findings of the extent of axonal injury in animal models of nerve injury and in humans with neuropathy [44–47] but in contrast to a study showing FA correlated with distal motor latency, thought to reflect myelin integrity [37]. Other discrepancies between DTI measures and function are evident from previous studies. Correlations between AD and nerve conduction velocities of the median nerve have been reported in patients with carpal tunnel syndrome [10, 48], suggesting that AD relates to integrity of myelin. On the contrary, a recent study in healthy subjects showed that AD of the median nerve correlated with compound motor action potentials (CMAP) amplitudes, presumed to relate to axon integrity [37]. Several possible explanations might explain these discrepancies. Firstly, it is possible that the relationships between DTI and neurophysiological measures are more complex, since single measures derived from DTI might not accurately reflect only one aspect of nerve structure (e.g. myelin or axonal integrity). Further, in patient populations, there will be structural changes due to pathology which are revealed as functional deficits. In healthy subjects, there is no such pathology, and the relationships found in patients might not be evident. Secondly, clinical neurophysiological findings do not always match symptoms. This again suggests that the relationships between structure and function of the nerves might be more complex and multi-faceted.

Evidence has shown that L5 and S1 nerve roots respond to neurophysiological testing differently. Previous work on the sensitivity of neurophysiological testing for each level of lumbar nerve root lesion found that the percentage of positive pathological results on EMG and in F-wave latencies were higher in L5 nerve root lesions than in S1 nerve root lesions [49]. This may also explain the correlation between neurophysiology, and DTI was not evident for the S1 nerve root but was found for the L5 nerve root. Alternatively, the

discrepancy in correlations could be explained by the lack of variability in our healthy subject data; the DTI data were consistent and the neurophysiological data were within normal ranges [50, 51]. It is therefore possible that associations might be revealed under pathological conditions, where changes in both neurophysiological and structural parameters are likely; a further study of the relationships between DTI metrics and neurophysiological measures in patients with compressed lumbar nerve roots is currently in progress.

In conclusion, the current findings provide a preliminary set of normative values of diffusion metrics for L5 and S1 nerve roots which suggests the potential for this DTI technique to be used in assessing lumbar spinal nerves in clinical settings as the values from the healthy subjects were highly consistent across the nerves of both sides as well as across levels. The relationships between DTI parameters and neurophysiological measures demonstrate the utility of using DTI metrics as a measure of nerve integrity and function. The current findings have clinical implications; the parameters derived from DTI provide quantitative information on lumbar spinal nerves which reflects their function. Whether these parameters can predict the likelihood of recovery of function following therapeutic interventions (e.g. surgery) in pathology remains to be established.

Compliance with ethical standards

Funding This study was funded by the Wellcome Trust Institutional Strategic Support Fund.

Conflict of interest The authors declare that they have no conflict of interest.

Ethical approval All procedures performed in studies involving human participants were in accordance with the ethical standards of the institutional and/or national research committee and with the 1964 Helsinki declaration and its later amendments or comparable ethical standards.

Informed consent Informed consent was obtained from all individual participants included in the study.

Open Access This article is distributed under the terms of the Creative Commons Attribution 4.0 International License (<http://creativecommons.org/licenses/by/4.0/>), which permits unrestricted use, distribution, and reproduction in any medium, provided you give appropriate credit to the original author(s) and the source, provide a link to the Creative Commons license, and indicate if changes were made.

References

- Alexander AL, Lee JE, Lazar M, Field AS (2007) Diffusion tensor imaging of the brain. *Neurotherapeutics* 4(3):316–329. doi:10.1016/j.nurt.2007.05.011
- Filippi M, Cercignani M, Inglese M, Horsfield MA, Comi G (2001) Diffusion tensor magnetic resonance imaging in multiple sclerosis. *Neurology* 56(3):304–311

3. Jayaram G, Stagg CJ, Esser P, Kischka U, Stinear J, Johansen-Berg H (2012) Relationships between functional and structural corticospinal tract integrity and walking post stroke. *Clin Neurophysiol* 123(12):2422–2428. doi:10.1016/j.clinph.2012.04.026
4. Hellyer PJ, Leech R, Ham TE, Bonnelle V, Sharp DJ (2013) Individual prediction of white matter injury following traumatic brain injury. *Ann Neurol* 73(4):489–499. doi:10.1002/ana.23824
5. Byblow WD, Stinear CM, Barber PA, Petoe MA, Ackerley SJ (2015) Proportional recovery after stroke depends on corticomotor integrity. *Ann Neurol* 78(6):848–859. doi:10.1002/ana.24472
6. Skorpil M, Karlsson M, Nordell A (2004) Peripheral nerve diffusion tensor imaging. *Magn Reson Imaging* 22(5):743–745. doi:10.1016/j.mri.2004.01.073
7. Hiltunen J, Suortti T, Arvela S, Seppa M, Joensuu R, Hari R (2005) Diffusion tensor imaging and tractography of distal peripheral nerves at 3 T. *Clin Neurophysiol* 116(10):2315–2323. doi:10.1016/j.clinph.2005.05.014
8. Khalil C, Hancart C, Le Thuc V, Chantelot C, Chechin D, Cotten A (2008) Diffusion tensor imaging and tractography of the median nerve in carpal tunnel syndrome: preliminary results. *Eur Radiol* 18(10):2283–2291. doi:10.1007/s00330-008-0971-4
9. Viallon A, Guyomarc'h S, Marjollet O, Berger C, Carricajo A, Robert F, Laporte S, Lambert C, Page Y, Zeni F, Bertrand JC (2008) Can emergency physicians identify a high mortality subgroup of patients with sepsis: role of procalcitonin. *Eur J Emerg Med* 15(1):26–33. doi:10.1097/MEJ.0b013e3280ec539b
10. Wang CK, Jou IM, Huang HW, Chen PY, Tsai HM, Liu YS, Lin CC (2012) Carpal tunnel syndrome assessed with diffusion tensor imaging: comparison with electrophysiological studies of patients and healthy volunteers. *Eur J Radiol* 81(11):3378–3383. doi:10.1016/j.ejrad.2012.01.008
11. Konstantinou K, Dunn KM (2008) Sciatica: review of epidemiological studies and prevalence estimates. *Spine (Phila Pa 1976)* 33(22):2464–2472. doi:10.1097/BRS.0b013e318183a4a2
12. Maniadas N, Gray A (2000) The economic burden of back pain in the UK. *Pain* 84(1):95–103
13. HCN (1999) Management of the lumbosacral radicular syndrome (sciatica). The Hague: Health Council of the Netherlands (18)
14. McGregor AH, Probyn K, Cro S, Dore CJ, Burton AK, Balague F, Pincus T, Fairbank J (2013) Rehabilitation following surgery for lumbar spinal stenosis. *Cochrane Database Syst Rev* 12:CD009644. doi:10.1002/14651858.CD009644.pub2
15. Ohnmeiss DD, Vanharanta H, Ekholm J (1997) Degree of disc disruption and lower extremity pain. *Spine (Phila Pa 1976)* 22(14):1600–1605
16. Thelander U, Fagerlund M, Friberg S, Larsson S (1992) Straight leg raising test versus radiologic size, shape, and position of lumbar disc hernias. *Spine (Phila Pa 1976)* 17(4):395–399
17. Facon D, Ozanne A, Fillard P, Lepeintre JF, Tournoux-Facon C, Ducreux D (2005) MR diffusion tensor imaging and fiber tracking in spinal cord compression. *AJNR Am J Neuroradiol* 26(6):1587–1594
18. Saritas EU, Cunningham CH, Lee JH, Han ET, Nishimura DG (2008) DWI of the spinal cord with reduced FOV single-shot EPI. *Magn Reson Med* 60(2):468–473. doi:10.1002/mrm.21640
19. Budzik JF, Vercllyte S, Lefebvre G, Monnet A, Forzy G, Cotten A (2013) Assessment of reduced field of view in diffusion tensor imaging of the lumbar nerve roots at 3 T. *Eur Radiol* 23(5):1361–1366. doi:10.1007/s00330-012-2710-0
20. Balbi V, Budzik JF, Duhamel A, Bera-Louville A, Le Thuc V, Cotten A (2011) Tractography of lumbar nerve roots: initial results. *Eur Radiol* 21(6):1153–1159. doi:10.1007/s00330-010-2049-3
21. Eguchi Y, Ohtori S, Yamashita M, Yamauchi K, Suzuki M, Orita S, Kamoda H, Arai G, Ishikawa T, Miyagi M, Ochiai N, Kishida S, Inoue G, Masuda Y, Ochi S, Kikawa T, Toyone T, Takaso M, Aoki Y, Takahashi K (2011) Diffusion-weighted magnetic resonance imaging of symptomatic nerve root of patients with lumbar disc herniation. *Neuroradiology* 53(9):633–641. doi:10.1007/s00234-010-0801-7
22. Chuanting L, Qingzheng W, Wenfeng X, Yiyi H, Bin Z (2014) 3.0T MRI tractography of lumbar nerve roots in disc herniation. *Acta Radiol* 55(8):969–975. doi:10.1177/0284185113508179
23. Wu W, Liang J, Ru N, Zhou C, Chen J, Wu Y, Yang Z (2016) Microstructural changes in compressed nerve roots are consistent with clinical symptoms and symptom duration in patients with lumbar disc herniation. *Spine (Phila Pa 1976)* 41(11):E661–E666. doi:10.1097/BRS.0000000000001354
24. Wahl M, Lauterbach-Soon B, Hattingen E, Jung P, Singer O, Volz S, Klein JC, Steinmetz H, Ziemann U (2007) Human motor corpus callosum: topography, somatotopy, and link between microstructure and function. *J Neurosci* 27(45):12132–12138. doi:10.1523/JNEUROSCI.2320-07.2007
25. Wilbourn AJ, Aminoff MJ (1998) AAEM minimonograph 32: the electrodiagnostic examination in patients with radiculopathies. *American Association of Electrodiagnostic Medicine. Muscle Nerve* 21(12):1612–1631
26. Barr K (2013) Electrodiagnosis of lumbar radiculopathy. *Phys Med Rehabil Clin N Am* 24(1):79–91. doi:10.1016/j.pmr.2012.08.011
27. Fisher MA (2002) Electrophysiology of radiculopathies. *Clin Neurophysiol* 113(3):317–335
28. Nagy Z, Weiskopf N (2008) Efficient fat suppression by slice-selection gradient reversal in twice-refocused diffusion encoding. *Magn Reson Med* 60(5):1256–1260. doi:10.1002/mrm.21746
29. Karampinos DC, Melkus G, Shepherd TM, Banerjee S, Saritas EU, Shankaranarayanan A, Hess CP, Link TM, Dillon WP, Majumdar S (2013) Diffusion tensor imaging and T2 relaxometry of bilateral lumbar nerve roots: feasibility of in-plane imaging. *NMR Biomed* 26(6):630–637. doi:10.1002/nbm.2902
30. Behrens TE, Woolrich MW, Jenkinson M, Johansen-Berg H, Nunes RG, Clare S, Matthews PM, Brady JM, Smith SM (2003) Characterization and propagation of uncertainty in diffusion-weighted MR imaging. *Magn Reson Med* 50(5):1077–1088. doi:10.1002/mrm.10609
31. Behrens TE, Berg HJ, Jbabdi S, Rushworth MF, Woolrich MW (2007) Probabilistic diffusion tractography with multiple fibre orientations: what can we gain? *NeuroImage* 34(1):144–155. doi:10.1016/j.neuroimage.2006.09.018
32. Inufusa A, An HS, Lim TH, Hasegawa T, Haughton VM, Nowicki BH (1996) Anatomic changes of the spinal canal and intervertebral foramen associated with flexion-extension movement. *Spine (Phila Pa 1976)* 21(21):2412–2420
33. Brefel-Courbon C, Payoux P, Ory F, Sommet A, Slaoui T, Raboyeau G, Lemesle B, Puel M, Montastruc JL, Demonet JF, Cardebat D (2007) Clinical and imaging evidence of zolpidem effect in hypoxic encephalopathy. *Ann Neurol* 62(1):102–105
34. Ayache SS, Creange A, Farhat WH, Zouari HG, Lesage C, Palm U, Abdellaoui M, Lefaucheur JP (2015) Cortical excitability changes over time in progressive multiple sclerosis. *Funct Neurol* 30(4):257–263
35. Miyagi R, Sakai T, Yamabe E, Yoshioka H (2015) Consecutive assessment of FA and ADC values of normal lumbar nerve roots from the junction of the dura mater. *BMC Musculoskelet Disord* 16:156. doi:10.1186/s12891-015-0576-4
36. Eguchi Y, Oikawa Y, Suzuki M, Orita S, Yamauchi K, Suzuki M, Aoki Y, Watanabe A, Takahashi K, Ohtori S (2016) Diffusion tensor imaging of radiculopathy in patients with lumbar disc herniation: preliminary results. *Bone Joint J* 98-B(3):387–394. doi:10.1302/0301-620X.98B3.36036
37. Heckel A, Weiler M, Xia A, Ruetters M, Pham M, Bendszus M, Heiland S, Baeumer P (2015) Peripheral nerve diffusion tensor

- imaging: assessment of axon and myelin sheath integrity. *PLoS One* 10(6):e0130833. doi:10.1371/journal.pone.0130833
38. Dallaudiere B, Lincot J, Hess A, Balbi V, Cornelis F, Larbi A, Laissy JP, Cotten A, Schouman-Claeys E (2014) Clinical relevance of diffusion tensor imaging parameters in lumbar disco-radicular conflict. *Diagn Interv Imaging* 95(1):63–68. doi:10.1016/j.diii.2013.08.019
 39. Shi Y, Zong M, Xu X, Zou Y, Feng Y, Liu W, Wang C, Wang D (2015) Diffusion tensor imaging with quantitative evaluation and fiber tractography of lumbar nerve roots in sciatica. *Eur J Radiol* 84(4):690–695. doi:10.1016/j.ejrad.2015.01.006
 40. Eisen A, Fisher M (1999) The F wave. *The International Federation of Clinical Neurophysiology. Electroencephalogr Clin Neurophysiol Suppl* 52:255–257
 41. Tievsky AL, Ptak T, Farkas J (1999) Investigation of apparent diffusion coefficient and diffusion tensor anisotropy in acute and chronic multiple sclerosis lesions. *AJNR Am J Neuroradiol* 20(8):1491–1499
 42. Werring DJ, Clark CA, Barker GJ, Thompson AJ, Miller DH (1999) Diffusion tensor imaging of lesions and normal-appearing white matter in multiple sclerosis. *Neurology* 52(8):1626–1632
 43. Field AS, Alexander AL (2004) Diffusion tensor imaging in cerebral tumor diagnosis and therapy. *Top Magn Reson Imaging* 15(5):315–324
 44. Mathys C, Aissa J, Meyer Zu Horste G, Reichelt DC, Antoch G, Turowski B, Hartung HP, Sheikh KA, Lehmann HC (2013) Peripheral neuropathy: assessment of proximal nerve integrity by diffusion tensor imaging. *Muscle Nerve* 48(6):889–896. doi:10.1002/mus.23855
 45. Lehmann HC, Zhang J, Mori S, Sheikh KA (2010) Diffusion tensor imaging to assess axonal regeneration in peripheral nerves. *Exp Neurol* 223(1):238–244. doi:10.1016/j.expneurol.2009.10.012
 46. Kakuda T, Fukuda H, Tanitame K, Takasu M, Date S, Ochi K, Ohshita T, Kohriyama T, Ito K, Matsumoto M, Awai K (2011) Diffusion tensor imaging of peripheral nerve in patients with chronic inflammatory demyelinating polyradiculoneuropathy: a feasibility study. *Neuroradiology* 53(12):955–960. doi:10.1007/s00234-010-0833-z
 47. Morisaki S, Kawai Y, Umeda M, Nishi M, Oda R, Fujiwara H, Yamada K, Higuchi T, Tanaka C, Kawata M, Kubo T (2011) In vivo assessment of peripheral nerve regeneration by diffusion tensor imaging. *J Magn Reson Imaging* 33(3):535–542. doi:10.1002/jmri.22442
 48. Lindberg PG, Feydy A, Le Viet D, Maier MA, Drape JL (2013) Diffusion tensor imaging of the median nerve in recurrent carpal tunnel syndrome—initial experience. *Eur Radiol* 23(11):3115–3123. doi:10.1007/s00330-013-2986-8
 49. Braune HJ, Wunderlich MT (1997) Diagnostic value of different neurophysiological methods in the assessment of lumbar nerve root lesions. *Arch Phys Med Rehabil* 78(5):518–520
 50. Puksa L, Stalberg E, Falck B (2003) Reference values of F wave parameters in healthy subjects. *Clin Neurophysiol* 114(6):1079–1090
 51. Claus D (1990) Central motor conduction: method and normal results. *Muscle Nerve* 13(12):1125–1132. doi:10.1002/mus.880131207